Mechanisms of EPR Hyperfine Coupling in Transition Metal Complexes

Markéta L. Munzarová,[†,‡] Pavel Kubáček,[†] and Martin Kaupp*[,‡]

Contribution from the Department of Theoretical and Physical Chemistry, Faculty of Science, Masaryk University, Kotlářská 2, CZ-61137 Brno, Czech Republic, and Institut für Anorganische Chemie, Universität Würzburg, Am Hubland, D-97074 Würzburg, Germany

Received June 9, 2000. Revised Manuscript Received August 25, 2000

Abstract: A detailed quantum chemical analysis of the underlying principles of hyperfine coupling in 3d transition metal complexes has been carried out. The explicit evaluation of one- and two-electron integrals for some atomic systems has been used to understand the spin polarization of the core shells. While spin polarization enhances the exchange interaction of the 2s and 2p shells with the singly occupied orbitals, the opposite spin polarization of the 3s and 3p shells arises from the required orthogonality to the 2s and 2p shells, respectively. Core-shell spin polarization in molecules is found to be proportional to the spin population in the valence 3d orbitals but to depend little on other details of bonding. In contrast, the spin polarization of the valence shell depends crucially on the overlap between the singly occupied and certain doubly occupied valence orbitals. Large overlap leads to pronounced spin polarization of these orbitals and, among other things, likely to spin contamination when using UHF wave functions or hybrid density functionals. The role of core- and valence-shell spin polarization for dipolar hyperfine couplings in transition metal complexes is discussed. It is demonstrated that great care should be exercised in deriving spin populations or even orbital compositions from dipolar couplings alone.

1. Introduction

The early history of EPR spectroscopy is closely connected to the study of transition metal complexes.[1−8] Already during the 1950s, the concept of spin polarization was used in the discussion of the hyperfine coupling constants (HFCCs) to transition metal nuclei (cf. section 2). Transition metal systems have thus been adequately represented in early, qualitative theoretical studies of EPR hyperfine couplings. In contrast, modern applications of quantum chemical methods to calculate hyperfine couplings more quantitatively have largely concentrated on organic radicals,[9,10] due to the various practical difficulties presented by the more complicated transition metal systems.[11]

We recently reported a systematic study,[11] in which various density functional theory (DFT) and coupled cluster approaches were critically compared in calculations of hyperfine coupling tensors for a representative set of 21 3d transition metal complexes. Complexes with significant metal 4s orbital contributions to the singly occupied molecular orbital(s) (SOMO) may be treated adequately with essentially any of the state-of-the-art density functionals. In contrast, it is much more difficult to reproduce experimentally derived HFC tensors in systems in which the spin density at the metal arises largely from spin polarization. Gradient-corrected functionals tend to underestimate the important spin polarization of the 2s and 3s core orbitals. While admixture of exact exchange in "hybrid functionals" helps to enhance the core-shell spin polarization in some cases, the related spin contamination may deteriorate significantly the quality of the results in other systems. Overall, no functional was found to perform satisfactorily for all systems, and for some systems, none of the functionals studied was acceptable.[11] The general quantitative study of HFC tensors for transition metal systems remains thus a challenge to quantum chemistry.

A better understanding of the detailed relation between electronic structure and hyperfine couplings should aid in looking for improved approaches for their calculation. Apart from the validation of existing methods, the detailed study of 21 complexes[11] has provided us with considerable qualitative insight into the mechanisms of spin polarization in transition metal systems. As expected, the underlying interactions can be much more variable than those in organic radicals. For example, not only s-type but also p- and d-type metal orbitals may be

* Corresponding author: (e-mail) kaupp@mail.uni-wuerzburg.de.
[†] Masaryk University.
[‡] Universität Würzburg.

(1) Abragam, A.; Bleaney, B. *Electron Paramagnetic Resonance of Transition Ions*; Clarendon Press: Oxford, 1970.
(2) Symons, M. C. R. *Chemical and Biochemical Aspects of Electron-Spin Resonance Spectroscopy*; Van Nostrand: New York, 1978.
(3) Atherton, N. M. *Principles of Electron Spin Resonance*; Prentice Hall: New York, 1993.
(4) Weil, J. A.; Bolton, J. R.; Wertz, J. E.; *Electron Paramagnetic Resonance: Elementary Theory and Practical Applications*; Wiley & Sons: New York, 1994.
(5) Carrington, A.; McLachlan, A. D. *Introduction to Magnetic Resonance with Applications to Chemistry and Chemical Physics*; Harper & Row: London, 1969.
(6) Weltner, W., Jr. *Magnetic Atoms and Molecules*; Van Nostrand: New York, 1983.
(7) McGarvey, B. R. In *Transition Metal Chemistry: A Series of Advances*; Carlin, R. L., Ed.; New York, 1966; Vol. 3, pp 89−201.
(8) Mabbs, F. E.; Collison, D. *Electron Paramagnetic Resonance of d Transition Metal Compounds*; Elsevier: Amsterdam, 1992.
(9) Engels, B.; Eriksson, L.; Lunell, S. *Adv. Quantum Chem.* **1996**, *27*, 297.
(10) Malkin, V. G.; Malkina, O. L.; Eriksson, L. A.; Salahub, D. R. In *Modern Density Functional Theory: A Tool for Chemistry*; Theoretical and Computational Chemistry Vol. 2; Politzer, P., Seminario, J. M., Eds.; Elsevier: Amsterdam, The Nederlands, 1995; pp 273−347.
(11) Munzarová M.; Kaupp, M. *J. Phys. Chem. A* **1999**, *103*, 9966.

10.1021/ja002062v CCC: $19.00
Published on Web 11/15/2000

involved, and both core and valence shells of the transition metal may be polarized significantly. The present work concentrates on these more qualitative aspects of hyperfine coupling in transition metal compounds and attempts to provide a detailed understanding of the different spin polarization mechanisms. Our interpretations are based on the molecular DFT calculations of ref 11 but will be augmented by detailed UHF and ROHF analyses of the relevant exchange, Coulomb, and one-electron integrals for some atomic systems. The geometrical and electronic structures of the molecular complexes studied, as well as the relevant available experimental data, have already been discussed.[11] Therefore, with the exception of few systems that will be discussed in more detail, the reader is referred to ref 11 for further information.

2. The Spin Polarization Model: Previous Work

The general theoretical background of EPR hyperfine coupling is documented in many textbooks.[1−8] The isotropic hyperfine coupling is directly proportional to the spin density at the point of the corresponding nucleus ($\rho_N^{\alpha-\beta}$, in the following abbreviated as ρ_N). In traditional interpretations, ρ_N is frequently approximated by the density of the singly occupied orbital(s). However, for the majority of systems studied by EPR spectroscopy, this simple approach is not sufficient. The unpaired electron, by virtue of its different interactions with electrons of different spin, spin-polarizes the electron distribution in the closed shells. This process can add significant spin density at the position of the nuclei. The inadequacy of the spin-restricted theory of the hyperfine interaction has been noted since 1933 for various main-group atoms.[12,13] In the 1950s, the spin polarization model turned out to be very important for the early qualitative interpretation of EPR spectra for the transition metal ions. In many of these, the unpaired electrons occupy metal d-type orbitals. Although these orbitals have a node at the nucleus, substantial isotropic hyperfine splittings from metal nuclei were observed. Abragam et al.[14] suggested that the isotropic hyperfine splitting in Mn^{2+} resulted from the spin polarization of the outermost occupied core shell (3s in the case of 3d metal ions).

Later, Watson and Freeman[15] showed by UHF calculations for several 3d ions that the polarized 2s shell contributes even more to the hyperfine coupling than the outermost 3s shell, but with the opposite (negative) sign.[16] Polarization of the 1s orbital provided also a negative, albeit very small, spin density at the nucleus. It was concluded that in the 1s and 2s shells, which exhibit radial density maximums at much smaller radii than the 3d orbital (cf. Figure 1), the α-spin electrons are "attracted" outward, leaving a region of negative spin density near the nucleus[17] (similar arguments have been used to describe the core polarization in 4d metal complexes[18]). The usual argument given is that exchange reduces the electron repulsion between $2s^\alpha$ and the $3d^\alpha$ SOMO and thus allows these electrons to get closer. This would correspond to an "effective attraction" of like-spin electrons. However, what happens with the 3s orbital? All of its radial maximums are also located closer to the nucleus than the 3d radial maximum (cf. Figure 1). Nevertheless, the 3s shell is polarized in the direction opposite from the 1s and 2s orbitals, as if the $3s^\alpha$ orbital were "repelled"[1] from the 3d-type SOMO. Watson and Freeman interpreted this as a result of the large overlap between 3s and 3d shells, leading to "competing tendencies" in the spin polarization.[15] We will show below that the requirement of orthogonality between 2s and 3s shells is responsible for these seemingly paradoxical observations.

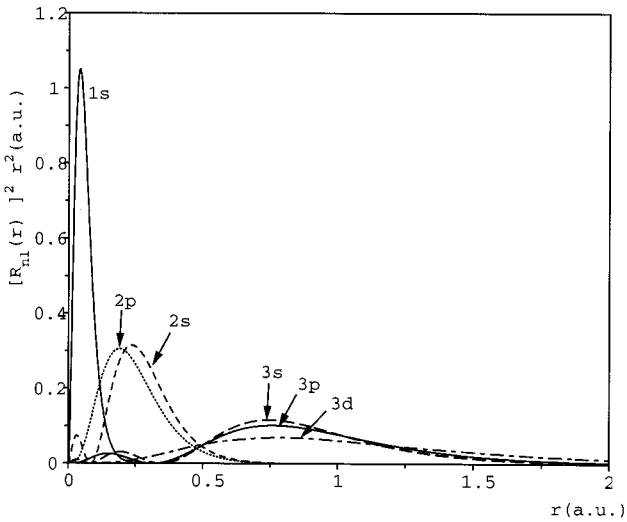

Figure 1. ROHF radial distribution functions $[R_{nl}(r)]^2r^2$ for Mn^{2+}.

In main-group chemistry, spin polarization dominates the hyperfine couplings for some 2p atoms and ions, for some small π-radicals (e.g., NO, CO^+, H_2O^+), and for the larger class of organic planar π-radicals. In these cases, the spin polarization of the 1s and 2s orbitals is known to transfer spin density to the nuclei. Just as for transition metal ions, spin polarization of the valence orbitals contributes with a positive sign to ρ_N, spin polarization of the core (1s) orbitals with a negative sign.[19,20] Unlike for transition metals, the positive outer-shell contributions dominate, providing an overall positive ρ_N.[21] The traditional interpretation of these observations is analogous to the model of Watson and Freeman. The α-component of the 1s orbital is attracted outward, leaving negative spin density at the nucleus. The $2s^\alpha$ orbital, which has its outermost maximum at slightly larger radius than 2p (Figure 2), is attracted inward and thus provides more α-spin density at the nucleus. This "exchange attraction" of electrons with the same spin is often viewed as a manifestation of Hund's rule of maximum multiplicity.[2,4]

In the past, the concept of spin polarization has been used exclusively to rationalize isotropic hyperfine couplings. However, recent theoretical work shows that dipolar hyperfine coupling in transition metal systems may also be influenced significantly by spin polarization.[11,22] In 3d complexes, large contributions to the metal dipolar coupling may come from the

(12) Fermi, E.; Segrè, E. *Rend. Accad. Nazl. Lincei* **1933**, *4*, 18; *Z. Phys.* **1933**, *82*, 729.
(13) Sternheimer, R. M. *Phys. Rev.* **1952**, *86*, 316.
(14) Abragam, A.; Horowitz, M.; Pryce, M. H. L. *Proc. R. Soc. A* **1955**, *230*, 169.
(15) Watson, R. E.; Freeman, A. J. *Phys. Rev.* **1961**, *123*, 2027.
(16) Negative contributions to ρ_N of metal 2s orbitals and positive contributions of metal 3s orbitals have been reported also: (a) Case, D. A.; Karplus, M. *J. Am. Chem. Soc.* **1977**, *99*, 6182. (b) Weber, J.; Goursot, A.; Pénigault, E.; Ammeter, J. H.; Bachmann, J. *J. Am. Chem. Soc.* **1982**, *104*, 1491.
(17) Freeman, A. J.; Watson, R. E. In *Magnetism*; Rado, G. T., Suhl, H., Eds.; Academic Press: NewYork, 1965; Vol. IIA, p 167.
(18) Watson, R. E.; Freeman, A. J. In *Hyperfine Interactions*, Freeman, A. J., Frankel, R. B., Eds.; Academic Press: NewYork, 1967; p 53.
(19) See, for example: (a) Karplus, M.; Fraenkel, G. K. *J. Chem. Phys.* **1961**, *35*, 1312. (b) Chang, S. Y.; Davidson, E. R.; Vincow, G. *J. Chem. Phys.* **1970**, *52*, 1741. (c) Chipman, D. M. *J. Chem. Phys.* **1983**, *78*, 3112. (d) Ishii, N.; Shimizu, T. *Phys. Rev. A* **1993**, *48*, 1691. (e) Engels, B.; Peyerimhoff, S. D. *Mol. Phys.* **1989**, *67*, 583.
(20) Chipman, D. M. *Theor. Chim. Acta* **1992**, *82*, 93.
(21) In contrast, the spin density at the hydrogen nuclei in planar π radicals is negative.[2,4]
(22) Belanzoni, P.; Baerends, E. J.; van Asselt, S.; Langewen, P. B. *J. Phys. Chem.* **1995**, *99*, 13094.

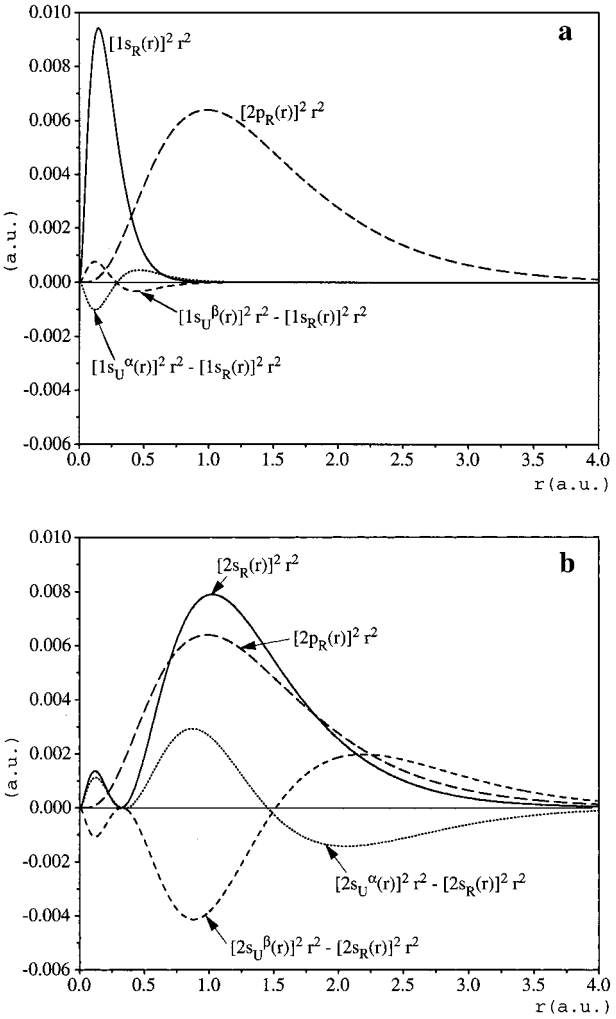

Figure 2. ROHF radial distribution functions $[R_{nl}(r)]^2r^2$, and differences between UHF and ROHF radial distributions in ^{4}N. (a) 1s (ROHF radial distribution scaled by $^1/_{30}$). (b) 2s (ROHF radial distribution scaled by $^1/_8$). For comparison, the ROHF radial distribution function of the 2p SOMOs (scaled by $^1/_8$) is also plotted (cf. discussion in section 5).

spin-polarized 2p and 3p orbitals. This viewpoint will be strengthened and extended to valence-shell contributions by the present work. Note that, for magnetic nuclei in an electronic environment of axial symmetry (i.e., those located on an at least 3-fold symmetry axis), as is the case for all transition metal nuclei studied here, the dipolar coupling tensor may be brought to the form $(-A_{dip}, -A_{dip}, 2A_{dip})$, where A_{dip} is the so-called dipolar hyperfine coupling constant.

3. Computational and Methodological Details

Calculations and MO Analyses of HFCCs. In the following discussion, we will neglect (spin−orbit or scalar) relativistic corrections to the HFCCs (which have been estimated in ref 11). The selection of experimental data for most of the systems used here, and the conversion between different representations of HFCCs, have been summarized in our previous work.[11] The computed and experimental molecular structures used are also those described in ref 11. We will concentrate on all-electron unrestricted Kohn−Sham calculations, mainly on results obtained with the gradient-corrected BP86[23] functional. This "pure" generalized gradient approximation has the advantage that spin contamination is typically very small.[11] Calculations and analyses of isotropic hyperfine coupling constants (at the Hartree−Fock and DFT level) were done with the Gaussian94 program.[24] Applying the CUBE program option, the values of the individual orbitals at the transition metal nuclei have been determined and they were used for the analysis of the contributions to ρ_N. DFT calculations of the dipolar hyperfine coupling constants have additionally been carried out with a modified version of the deMon-EPR code,[10,25] where a routine for the analysis of the orbital contributions to A_{dip} has been implemented.

The medium-sized (15s11p6d)/[9s7p4d] metal basis sets constructed in ref 11 (based on the work of Schäfer et al.[26]) were used together with basis sets BIII of Kutzelnigg et al. (also known as IGLO-III[27]) for main-group atoms. In the Gaussian94 DFT calculations, the default integration grids (int = finegrid option[24]) of the program have been used. In deMon calculations, additional auxiliary basis sets (5,5;5,5) for the metal and (5,2;5,2) for the ligand have been used to fit the density and the exchange-correlation potential (in this case, an extra iteration without fit of the potential and with extended grid was carried out after SCF convergence). For the numerical integration in deMon, we have employed a nonrandom FINE angular grid with 128 radial shells.[10,28]

Hartree−Fock Analysis of One- and Two-Electron Integrals. The total energy corresponding to a Hartree−Fock wave function may be written as[29]

$$E_0 = \sum_i^{N^\alpha} h_{ii}^{\alpha} + \sum_i^{N^\beta} h_{ii}^{\beta} + \frac{1}{2}\sum_i^{N^\alpha}\sum_j^{N^\alpha}(J_{ij}^{\alpha\alpha} - K_{ij}^{\alpha\alpha}) + \frac{1}{2}\sum_i^{N^\beta}\sum_j^{N^\beta}(J_{ij}^{\beta\beta} - K_{ij}^{\beta\beta}) + \sum_i^{N^\alpha}\sum_j^{N^\beta} J_{ij}^{\alpha\beta} \quad (1)$$

with α and β denoting spin.

The one-electron term

$$h_{ii} = \int d\mathbf{r}_1 \psi_i^*(\mathbf{r}_1)\left(-\frac{1}{2}\nabla_1^2 - \sum_A \frac{Z_A}{\mathbf{r}_{1A}}\right)\psi_i(\mathbf{r}_1) \quad (2)$$

represents the average kinetic and nuclear-attraction energy of an electron described by the orbital $\psi_i(\mathbf{r}_1)$; the two-electron Coulomb integral

$$J_{ij} = \langle ij|ij\rangle = \int d\mathbf{r}_1\, d\mathbf{r}_2 |\psi_i(\mathbf{r}_1)|^2 \mathbf{r}_{12}^{-1} |\psi_j(\mathbf{r}_2)|^2 \quad (3)$$

expresses the classical Coulomb repulsion between the charge

(23) Perdew, J. P.; Wang, Y. *Phys. Rev. B* **1986**, *33*, 8822. Perdew, J. P.; Wang, Y. *Phys. Rev. B* **1986**, *34*, 7406.

(24) Frisch, M. J.; Trucks, G. W.; Schlegel, H. B.; Gill, P. M. W.; Johnson, B. G.; Robb, M. A.; Cheeseman, J. R.; Keith, T.; Petersson, G. A.; Montgomery, J. A.; Raghavachari, K.; Al-Laham, M. A.; Zakrzewski, V. G.; Ortiz, J. V.; Foresman, J. B.; Peng, C. Y.; Ayala, P. Y.; Chen, W.; Wong, M. W.; Andres, J. L.; Replogle, E. S.; Gomperts, R.; Martin, R. L.; Fox, D. J.; Binkley, J. S.; Defrees, D. J.; Baker, J.; Stewart, J. P.; Head-Gordon, M.; Gonzalez, C.; Pople, J. A. *Gaussian 94* (revision E.2); Gaussian, Inc.: Pittsburgh, PA, 1995.

(25) a) Salahub, D. R.; Fournier, R.; Mlynarski, P.; Papai, I.; St-Amant, A.; Ushio, J. In *Density Functional Methods in Chemistry*; Labanowski, J., Andzelm, J., Eds.; Springer: New York, 1991. (b) St-Amant, A.; Salahub, D. R. *Chem. Phys. Lett.* **1990**, *169*, 387.

(26) Schäfer, A.; Horn, H.; Ahlrichs, R. *J. Chem. Phys* **1992**, *97*, 2571.

(27) Kutzelnigg, W.; Fleischer, U.; Schindler, M. In *NMR−Basic Principles and Progress*; Vol. 23, Springer-Verlag: Heidelberg, 1990; Vol. 23, p 165.

(28) Daul, C. A.; Goursot, A.; Salahub, D. R. In *NATO ARW Proceedings on Grid Methods in Atomic and Molecular Quantum Calculation*; Vol. C412, Cerjan, C., Ed.; Kluwer: Dordrecht, 1993; Vol. C412.

(29) Szabo, A.; Ostlund, Neil S. *Modern Quantum Chemistry*; Dover: New York, 1996.

Table 1. Spin Densities at the Metal Nuclei (au) for a Series of Manganese Complexes[a]

	contributions[b]							
	core							
molecule	1s	2s	3s	VS	SOMO	total	exp[c]	3s/2s
$^2[Mn(CO)_5]$	0.00	−0.18	0.09	0.04	0.06	0.00	0.00...0.01	−0.50
$^2MnO_3$	0.01	−0.33	0.18	−0.58	2.54	1.82	1.46	−0.55
$^2[Mn(CN)_4N]^-$	0.00	−0.39	0.20	0.04	0.00	−0.15	−0.25	−0.51
$^2[Mn(CN)_5NO]^{2-}$	−0.01	−0.50	0.24	0.13	0.00	−0.13	−0.20	−0.48
^6MnO	0.01	−1.40	0.64	−0.43	3.56	2.39	2.17	−0.46
$^6[Mn(CN)_4]^{2-}$	−0.03	−1.60	0.71	0.46	0.00	−0.45	−0.60	−0.44
$^6MnF_2$	0.00	−1.62	0.72	−0.22	2.45	1.33	0. 47...0.61	−0.44
^7MnH	0.01	−1.69	0.72	−0.84	3.86	2.07	1.52	−0.43
^7MnF	0.01	−1.70	0.74	−0.12	3.68	2.61	2.40	−0.44
^6Mn	−0.01	−1.78	0.78	0.93	0.00	−0.07	−0.35[d]	−0.44
$^7Mn^+$	0.04	−1.79	0.76	0.00	5.30	4.31	4.12	−0.43
$^6Mn^{2+}$	−0.01	−1.85	0.79	0.00	0.00	−1.07	−0.76...−1.24[e]	−0.43

[a] DFT results with the BP86 functional. [b] Contributions from the core-shell spin polarization (1s,2s,3s), valence-shell spin polarization (VS), and singly occupied orbital(s) (SOMO). [c] From ref 11, unless stated otherwise. [d] Kasai, P. H. *Acc. Chem. Res.* **1971**, *4*, 329. Ar-matrix isolation. [e] Values obtained in different host crystals; see ref 1.

Table 2. Spin Densities at the Metal Nuclei (au) for a Series of First-Row Transition Metal Complexes[a]

	contributions[b]							
	core							
molecule	1s	2s	3s	VS	SOMO	total	exp[c]	3s/2s
^3TiO	0.03	−0.24	0.02	−0.12	2.31	1.99	1.91	−0.08
$^2TiF_3$	0.01	−0.17	0.03	−0.09	1.07	0.86	0.70...0.73	−0.18
^3VN	0.03	−0.34	0.07	−0.27	2.87	2.37	2.23	−0.21
^4VO	0.02	−0.58	0.17	−0.25	2.74	2.09	1.98	−0.29
$^6Cr^+$	0.00	−1.38	0.42	0.00	0.00	−0.97		−0.30
$^6[Cr(CO)_4]^+$	−0.01	−1.20	0.39	0.35	0.00	−0.47	−0.82	−0.33
$^6Fe^{3+}$	−0.03	−2.30	1.19	0.00	0.00	−1.14	−0.81...−1.05[d]	−0.52
$^2[Fe(CO)_5]^+$	−0.01	−0.33	0.19	0.05	0.10	0.00	−0.02	−0.58
$^2[Co(CO)_4]$	0.00	−0.38	0.23	0.05	0.10	0.00	−0.05	−0.61
$^2[Ni(CO)_3H]$	−0.02	−0.18	0.12	0.00	0.01	−0.06	−0.02	−0.67

[a] DFT results with the BP86 functional. [b] Contributions from the core-shell spin polarization (1s,2s,3s), valence-shell spin polarization (VS), and singly occupied orbital(s) (SOMO). [c] From ref 11, unless stated otherwise. [d] Values obtained in different host crystals; see ref 1.

clouds $|\psi_i(\mathbf{r}_1)|^2$ and $|\psi_j(\mathbf{r}_2)|^2$; the two-electron exchange integral

$$K_{ij} = \langle ij|ji\rangle = \int d\mathbf{r}_1\, d\mathbf{r}_2 \psi_i^*(\mathbf{r}_1)\psi_j(\mathbf{r}_1) r_{12}^{-1} \psi_j^*(\mathbf{r}_2)\psi_i(\mathbf{r}_2) \quad (4)$$

represents the exchange correlation of the two electrons ($\mathbf{r}_i$ denotes the coordinates of electron i).[30]

At the unrestricted Hartree−Fock (UHF) level of theory, the spatial parts of the ψ_i^α and ψ_i^β orbitals are allowed to differ, while at the restricted-open-shell Hartree−Fock (ROHF) level they are required to be identical for every $i \le N^\beta$. In the following, we will discuss also the overlap integral

$$S_{ij} = \langle i|j\rangle = \int d\mathbf{r} \psi_i^*(\mathbf{r})\psi_j(\mathbf{r}) \quad (5)$$

UHF and ROHF wave functions have been compared in terms of energies and spin density distributions for a number of spherical $3d^5$ cations (Cr^+, Mn^{2+}, Fe^{3+}), and for the nitrogen atom, using the Gaussian94 code, and basis sets as described above. Using the CUBE option, the radial wave functions have been extracted. Applying standard methods of two-electron integral calculations for atomic systems,[31] the values of Coulomb and exchange integrals, nuclear attraction integrals, and overlap between radial wave functions (cf. below) have been determined. For the numerical calculation of the Slater−Condon parameters, a radial grid of 10^{-3} au has been employed over a radius of 10 au from the nucleus. Summation over all electrons and pairs of electrons gives the total nuclear attraction energy and electron repulsion energy (cf. eq 1). The total kinetic energy has been extracted from the Gaussian94 output.

Below we refer to the sum of all Coulomb integrals from eq 1 as the total Coulomb energy (E_C) and to the sum of all exchange integrals from eq 1 as the total (negative) exchange energy (E_X). Note that the summations in eq 1 are not restricted to pairs of different spin−orbitals. Therefore, the (unphysical) electrostatic interaction of an electron with itself is accounted for in the Coulomb part and again subtracted in the exchange part (ref 32 p 180). This allows a unique orbital breakdown of the total electron repulsion energy into exchange and Coulomb parts.[33] The Coulomb part may be interpreted as a classical electrostatical energy of a charge cloud of density $\rho(r)$, whereas the exchange part includes all nonclassical effects, (ref 32, pp 34 and 39).

4. Analysis of Contributions to ρ_N

Table 1 gives a breakdown of the DFT results for the spin density at the metal nucleus into MO contributions in a series of manganese complexes (and in three atomic systems). Table

(30) In this work, the notation for one- and two-electron integrals pertains to integration over the spatial parts of the corresponding spin−orbitals only.

(31) Weissbluth, M. *Atoms and Molecules*; Academic Press: New York, 1980.

(32) Parr, R. G.; Yang, W. *Density-functional theory of atoms and molecules*; Oxford University Press: New York, 1989.

(33) When self-interaction is not accounted for, the decomposition of electron repulsion energy into Coulomb and exchange parts may be arbitrary. For example, for a p shell fully occupied with six electrons, both the total Coulomb and the total exchange energy depend on the orbital basis (angular momentum eigenfunctions or real functions). The reason is that $\langle p_x p_y|p_x p_y\rangle = \langle p_x p_z|p_x p_z\rangle = \langle p_y p_z|p_y p_z\rangle = \langle p_1 p_0|p_1 p_0\rangle = \langle p_{-1} p_0|p_{-1} p_0\rangle \neq \langle p_{-1} p_1|p_{-1} p_1\rangle$. An analogous relation holds for the corresponding exchange integrals.

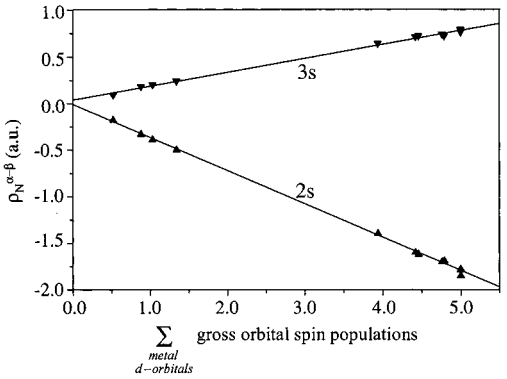

Figure 3. Correlation between Mulliken gross d-orbital spin populations and core-shell spin polarization for a series of manganese complexes. BP86 results.

2 provides the same analysis for other 3d complexes. In addition to the 1s, 2s, and 3s core contributions (i.e., contributions from MOs with predominantly metal core character), we summarize under "valence" contributions arising from the spin polarization of the doubly occupied valence MOs. The direct contribution(s) from the SOMO(s) is(are) also given (for cases such as MnH or MnF_2, where more than one SOMO possesses s-character, their contributions have been summed up). Spin densities derived from experimental hyperfine coupling constants[11] are included for comparison.

While contributions from valence-shell spin polarization vary in both their signs and magnitudes, the core contributions depend much less on the detailed bonding situation (compare, e.g., $[Mn(CN)_4]^{2-}$ and MnF_2).[34] The negative 2s contributions dominate, whereas the 3s contributions are smaller and positive. The 1s contributions are very small. Both 2s and 3s contributions increase with increasing spin multiplicity of the system. However, the ratio between 3s and 2s (3s/2s ratio in Tables 1 and 2) remains close to −0.5 for all Mn complexes (Table 1). A more detailed analysis indicates that both the 2s and 3s contributions exhibit a remarkable proportionality to the total 3d spin population (Figure 3). Neither the specific bonding situation nor the spin population of the metal 4s orbitals influence the 2s and 3s contributions appreciably. For example, we may compare the 2s and 3s contributions to ρ_N for the ^6Mn atom (−1.78 and 0.78 au), the $^7Mn^+$ cation (−1.79 and 0.76 au), and the $^6Mn^{2+}$ cation (−1.85 and 0.79 au).

Interestingly, the 3s/2s ratio is influenced more by nuclear charge than by anything else (Tables 1 and 2). It becomes more negative when moving toward the right end of the 3d series. This is seen best when comparing the isoelectronic high-spin d^5 ions $^6Cr^+$, $^6Mn^{2+}$, and $^6Fe^{3+}$, for which the 3s/2s ratio is computed to be −0.30, −0.43, and −0.52, respectively. Intuitively, it is not clear whether this is just a consequence of a change in the relative magnitudes of the (spin-averaged) 3s and 2s orbitals at the nucleus or of an increasing spin polarization of the 3s orbital with increasing nuclear charge. As will be shown below, the latter interpretation is to be preferred. In the following, the spatial parts of the spin−orbitals $\psi^{\alpha}_{2s}(\mathbf{r})\alpha(\sigma)$, $\psi^{\beta}_{2s}(\mathbf{r})\beta(\sigma)$, $\psi^{\alpha}_{3s}(\mathbf{r})\alpha(\sigma)$, and $\psi^{\beta}_{3s}(\mathbf{r})\alpha(\sigma)$ will be abbreviated as $2s^{\alpha}(r)$, $2s^{\beta}(r)$, $3s^{\alpha}(r)$, and $2s^{\beta}(r)$, respectively (subscripts U and R will indicate unrestricted or restricted orbitals). For s-type orbitals, the angular part of the wave function is constant and equal to 1. Therefore, we will in the following refer to the radial wave functions only (hence, the scalar argument r is used, rather than the vector $\mathbf{r}$). A given pair of spin-polarized orbitals $2s^{\alpha}_U$ and $2s^{\beta}_U$ contributes to ρ_N like $(2s^{\alpha}_U(0))^2 - (2s^{\beta}_U(0))^2$. The function $(2s^{\alpha}_U(\mathbf{r}))^2 - (2s^{\beta}_U(\mathbf{r}))^2$ may be divided into two parts corresponding to (i) the polarization of the $2s^{\alpha}$ orbital and (ii) the polarization of the $2s^{\beta}$ orbital, relative to the corresponding orbitals in the restricted (Hartree−Fock or Kohn−Sham) calculation. We may thus expand the function as

$$(2s^{\alpha}_U(r))^2 - (2s^{\beta}_U(r))^2 = [(2s^{\alpha}_U(r))^2 - (2s_R(r))^2] + [(2s_R(r))^2 - (2s^{\beta}_U(r))^2] = [2s^{\alpha}_U(r) + 2s_R(r)][2s^{\alpha}_U(r) - 2s_R(r)] + [2s_R(r) + 2s^{\beta}_U(r)][2s_R(r) - 2s^{\beta}_U(r)] \quad (6)$$

If we denote $[2s^{\alpha}_U(r) - 2s_R(r)]$ as $\Delta 2s^{\alpha}$ and $[2s^{\beta}_U(r) - 2s_R(r)]$ as $\Delta 2s^{\beta}$, eq 6 may be rewritten as

$$(2s^{\alpha}_U(r))^2 - (2s^{\beta}_U(r))^2 = [2(2s_R(r)) + \Delta 2s^{\alpha}(r)]\Delta 2s^{\alpha}(r) - [2(2s_R(r)) + \Delta 2s^{\beta}(r)]\Delta 2s^{\beta}(r) = 2(2s_R(r))(\Delta 2s^{\alpha}(r) - \Delta 2s^{\beta}(r)) + (\Delta 2s^{\alpha}(r))^2 - (\Delta 2s^{\beta}(r))^2 \quad (7)$$

Both $\Delta 2s^{\alpha}(r)$ and $\Delta 2s^{\beta}(r)$ are much smaller than $2s_R(r)$. The quadratic terms $(\Delta 2s^{\alpha}(r))^2$, $(\Delta 2s^{\beta}(r))^2$ may therefore be neglected. Furthermore, to a large extent $(\Delta 2s^{\alpha}(r))^2$ is compensated by $-(\Delta 2s^{\beta}(r))^2$ (cf. section 5). The left side of eq 7 may thus be approximated as

$$(2s^{\alpha}_U(r))^2 - (2s^{\beta}_U(r))^2 \approx 2(2s_R(r))(\Delta 2s^{\alpha}(r) - \Delta 2s^{\beta}(r)) \quad (8)$$

Analogously we obtain for the contribution from the 3s orbitals

$$(3s^{\alpha}_U(r))^2 - (3s^{\beta}_U(r))^2 \approx 2(3s_R(r))(\Delta 3s^{\alpha}(r) - \Delta 3s^{\beta}(r)) \quad (9)$$

The ratio between the 3s and 2s orbital contributions is thus to a good approximation

$$\frac{(3s^{\alpha}_U(r))^2 - (3s^{\beta}_U(r))^2}{(2s^{\alpha}_U(r))^2 - (2s^{\beta}_U(r))^2} \approx \frac{3s_R(r)}{2s_R(r)} \frac{\Delta 3s^{\alpha}(r) - \Delta 3s^{\beta}(r)}{\Delta 2s^{\alpha}(r) - \Delta 2s^{\beta}(r)} \quad (10)$$

Each of the orbital contributions to $\rho^{\alpha-\beta}(r)$ is therefore roughly proportional to the difference between the restricted and unrestricted orbitals, but also to the absolute value of the restricted orbital. As a consequence, the much larger value of the 2s orbital at the nucleus results in the larger 2s orbital contribution to $\rho^{\alpha-\beta}(0)$, although $\Delta 3s^{\alpha}(0) - \Delta 3s^{\beta}(0) > \Delta 2s^{\alpha}(0) - \Delta 2s^{\beta}(0)$. The ratio $3s_R(0)/2s_R(0)$ changes only slightly throughout the 3d series: for Cr^+, Mn^{2+}, and Fe^{3+}, we obtain the ratios −0.373, −0.377, and −0.383, respectively (BP86 results). In contrast, $\Delta 3s^{\alpha}(0) - \Delta 3s^{\beta}(0)/\Delta 2s^{\alpha}(0) - \Delta 2s^{\beta}(0)$ changes from −0.821 for Cr^+ through −1.138 for Mn^{2+}, to −1.348 for Fe^{3+} (extracted from ROBP86 and UBP86 results). An interpretation of this trend is given in section 5.

While the valence-shell spin polarization contributions to ρ_N appear to be irregular at first sight, we find a relation between their sign and the character of the SOMO: The valence contribution to ρ_N is positive only when there is no metal 4s admixture into the SOMO (e.g., in $^6Mn^0$, $^6[Mn(CN)_4]^{2-}$, $^6[Cr(CO)_4]^+$) or when the admixture is very small ($^2[Mn(CO)_5]$, $^2[Fe(CO)_5]^+$).[35] In the presence of significant metal 4s contribu-

(34) The low sensitivity of spin polarization contributions to ρ_N in organic radicals on the particular bonding situation has been discussed. The proportionality between the 1s and 2s contributions for CH_3 over a wide range of conditions (out-of-plane bending) has also been reported.

(35) For main-group systems with 2p-type SOMOs, that for symmetry reasons may not mix with the bonding MOs, valence-shell spin polarization always contributes positively to ρ_N (at the given main-group center).[19]

Table 3. Spin Densities at the Metal Nuclei (au) for a Series of Atomic Systems with Five Singly Occupied 3d Orbitals[a]

	contribution[b]							
	core							
atom/ion	1s	2s	3s	VS	SOMO	total	exp[c]	3s/2s
$^6Cr^+$	−0.04	−2.11	0.51	0.00	0.00	−1.64		−0.24
^6Mn	−0.04	−2.71	1.31	1.08	0.00	−0.36	−0.33	−0.48
$^6Mn^{2+}$	−0.08	−2.82	1.34	0.00	0.00	−1.57	−1.24...−0.76	−0.48
$^6Fe^{3+}$	−0.12	−3.56	2.21	0.00	0.00	−1.48	−0.81...−1.05	−0.62

[a] UHF results. [b] Contributions from the core-shell spin polarization (1s,2s,3s), valence-shell spin polarization (VS), and singly occupied orbital(s) (SOMO). [c] Cf. Tables 1 and 2 for references.

tions to the SOMO (and thus of large direct, positive SOMO contributions to ρ_N), the spin polarization of the valence shell always contributes negatively to ρ_N (cf. MnH, MnO, MnO_3, and TiF_3 in Tables 1 and 2).

The signs of the individual MO contributions in Tables 1 and 2 remain the same with the other gradient-corrected and hybrid functionals compared in ref 11, or even at the UHF level. From a quantitative point of view, the contributions change only relatively little for different correlation functionals tested but change significantly upon inclusion of Hartree−Fock exchange into the exchange functional. This is easily understandable, as UHF calculations overestimate spin polarization considerably and thus lead to much larger negative core-shell contributions to ρ_N. In contrast, gradient-corrected functionals tend to underestimate the core-shell spin polarization.[11] Admixture of (the right amount of) Hartree−Fock exchange frequently brings the results into better agreement with experiment. Negative contributions from valence-shell spin polarization are also often overestimated at the UHF level. In all cases studied, the UHF spin densities at the metal are lower than the DFT results (due to the core-shell contributions) and too low compared to experiment (cf. ref 11).

As an example, UHF results for a series of atomic high-spin d^5 systems are shown in Table 3. All qualitative aspects (sign and relative magnitude of the orbital contributions) are the same for UHF as for DFT (BP86, cf. Tables 1 and 2). We note that the increase in the 3s/2s ratio along the 3d series (cf. discussion above) is also present, albeit somewhat overestimated, at the UHF level. Referring to eq 10, $3s_R(0)$ /$2s_R(0)$ changes from −0.362 for Cr^+ through −0.367 for Mn^{2+} to −0.373 for Fe^{3+}, and $\Delta 3s^\alpha(0) - \Delta 3s^\beta(0)$ /$\Delta 2s^\alpha(0) - \Delta 2s^\beta(0)$ changes from −0.667 for Cr^+, through −1.290 for Mn^{2+}, to −1.348 for Fe^{3+} (ROHF and UHF results, respectively). The qualitative similarity of the DFT and HF results justifies our use, in the following section 5, of HF wave functions in the detailed analysis of spin polarization in atoms. We note that spin contamination is negligible for the high-spin atomic systems studied, even with UHF wave functions.

5. Analysis of Spin Polarization in Atomic Systems

We will start our discussion with a comparison of spin-restricted and spin-polarized orbitals for Mn^{2+}. In its $^6Mn^{2+}$ ground state, the cation has five unpaired electrons, all of them occupying metal 3d orbitals. The maximum of the 3d radial distribution is located at only slightly larger radius than the outermost maximums of the doubly occupied 3s and 3p semicore orbitals (Figure 1). The 2s and 2p orbitals are much more contracted and well separated from the M shell.

Spin Polarization of 2s **vs** 3s **and** 2p **vs** 3p **Core Shells.** Panels a−d of Figure 4 show radial distributions of the 2s, 2p, 3s, and 3p ROHF orbitals of $^6Mn^{2+}$, respectively, as well as the associated differences between the UHF and ROHF distributions. The area confined between $[\psi_U(r)]^2r^2 - [\psi_R(r)]^2r^2$ and the x axis may be interpreted as a measure of spin-density redistribution within a given spin−orbital, due to spin polarization. We find that (a) in areas where the spin polarization increases the magnitude of the α spin−orbital, the magnitude of the corresponding β spin−orbital is decreased and vice versa; (b) close to the nucleus (within ∼0.3 au), the spin density of the $2s^\alpha$ orbital decreases whereas that of the $3s^\alpha$ orbital increases (see Figure 4a,c). The same holds for the relation between the $2s^\beta$ and $3s^\beta$ curves. Furthermore, the $2p^\alpha$ and $3p^\alpha$ curves, as well as the $2p^\beta$ and $3p^\beta$ curves, exhibit the same kind of complementarity in the core region (cf. Figure 4b,d). This suggests that the relation between the 2s and 3s contributions to ρ_N, in particular their opposite sign (as well as the relation between 2p and 3p contributions to the dipolar coupling, cf. section 7), is due to the orthogonality required between the orbitals of the M and L shells.

To gain deeper insight into this relation, we examine in Table 4 the influence of spin polarization on the values of two-electron integrals between the SOMO(s) and the (spin-polarized) doubly occupied orbitals. We discuss first the exchange integrals. Each of them has been calculated (a) for both electrons occupying ROHF orbitals, (b) for the unpaired electron in a ROHF orbital and the "paired" electron in a UHF orbital, and (c) for both electrons in spin-relaxed (unrestricted) orbitals. This allows us to compare the energy gain/loss due to the spin polarization of the doubly occupied orbital and the effect of the relaxation (contraction) of the SOMO. The spin polarization of the 2s and 2p orbitals increases their exchange interaction with the SOMO, and the SOMO relaxation enhances this interaction further, so that the exchange stabilization may be understood as a driving force of 2s and 2p spin polarization. Exchange stabilization correlates with an increase in the overlap of the radial wave functions (Table 4, Figure 4a,b). In the following, we will refer to this type of overlap integral as *radial overlap*, as opposed to the more common overlap integral defined in eq 5. The exchange of the 3s or 3p orbitals with the 3d SOMO is decreased by core-shell spin polarization and is accompanied by a decrease in the radial overlap (Table 4). Relaxation of the SOMO recovers only part of the radial overlap and of the exchange interaction. Obviously, the redistribution of spin density does not enhance the exchange interaction with the SOMO for all orbitals.

This may be not too surprising, as not only exchange with the SOMO but also Coulomb repulsion with the SOMO, exchange and Coulomb repulsion with the other electrons, and electron−nuclear attraction and kinetic energy change upon going from the ROHF to the UHF wave function. Indeed, the absolute value of the exchange energy is roughly 1 order of magnitude smaller than these other terms. Note, also, that changes in the exchange and Coulomb interactions for the α spin−orbital are partly compensated by the corresponding, complementary changes in the β component (Table 4). Spin polarizations of individual orbitals are obviously not independent processes.

What is the driving force for the spin polarization of the 3s (and 3p) orbitals? To understand this we have to be aware that the optimized orbitals for an atom have to be orthogonal. This may be realized (a) by the spin parts, (b) by the angular parts, or (c) by the radial parts of the wave functions. For two s-type α spin−orbitals, condition c applies; i.e., the radial functions have to be orthogonal, both for the ROHF and UHF wave functions. In other words, the area between the function $f =$

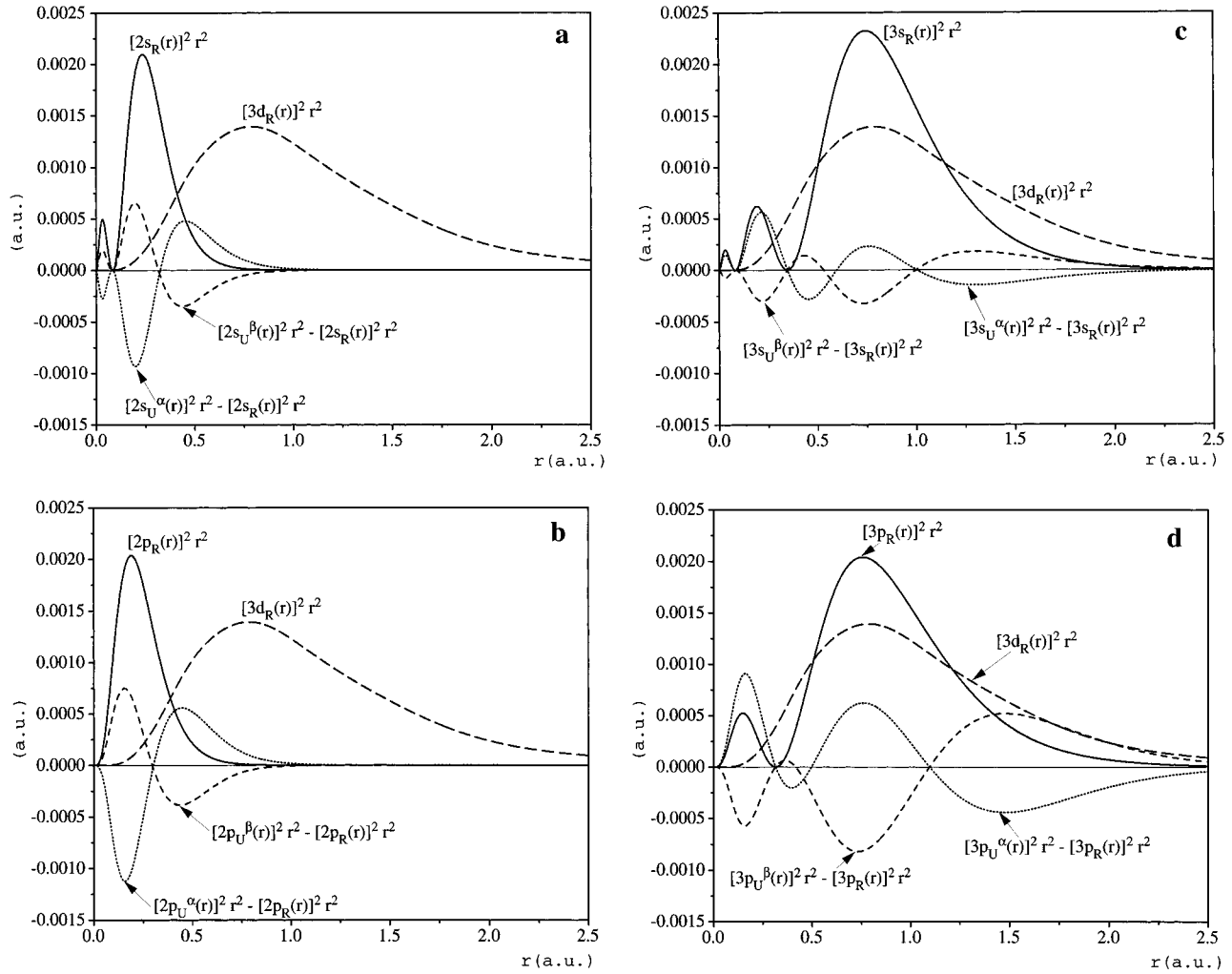

Figure 4. ROHF radial distribution functions $[R_{nl}(r)]^2r^2$ (scaled by $^1/_{150}$), and difference between UHF and ROHF radial distributions for Mn^{2+}. (a) 2s, (b) 2p, (c) 3s, (d) 3p. For comparison, the ROHF radial distribution function of the singly occupied 3d orbitals (scaled by $^1/_{50}$) is also shown. See text also.

$2s(r)3s(r)\ r^2$ and the x axis in regions where f is positive has to be equal to the area in regions where f is negative. This is demonstrated in Figure 5 for the spin-restricted case. If we now, for example, allow the $2s^\alpha$ orbital to be polarized (decontracted to larger r, cf. Figure 4a), the negative area under f decreases, whereas the positive area increases. The orthonormality between $2s^\alpha$ and $3s^\alpha$ has been lost. To recover it, the polarization of the $3s^\alpha$ orbital must again enhance the negative area and reduce the positive area; i.e., it has to contract. Changes of the $2s^\beta$ and $3s^\beta$ spin−orbitals behave analogously, with opposite directions. The same conditions apply to the $2p^\alpha/3p^\alpha$ and $2p^\beta/3p^\beta$ pairs; i.e., their radial functions must also remain orthogonal. Thus, orthogonality requires complementary polarizations of the L and M shells. This orthogonality does not hold strictly for molecular systems. However, as the nature of the core orbitals does not change much in molecules, we expect that the same mechanisms apply (see further below).

From this we conclude that the 2s orbital is spin-polarized to enhance the exchange interaction with the SOMO. The 3s orbital has to stay orthogonal on 2s, even if this means a reduced exchange interaction with the SOMO. Why does the spin polarization of the 2s orbital dominate? The reason is that the energy gain in the exchange interaction between the 2s and the 3d SOMO is much larger than the energy loss due to the exchange interaction between the 3s and the 3d SOMO (Table 4). If we were to optimize the exchange between 3s and the SOMO, the reduced exchange interaction between 2s and the SOMO would overcompensate the gain. This is best illustrated in Figure 4. $2s^\alpha$ is well separated from 3d and clearly enhances its interaction with the SOMO upon radial expansion (Figure 4a). In contrast, spin polarization of $3s^\alpha$ is much less effective, as areas with increased and reduced overlap will partly compensate each other (Figure 4c). The same arguments may be applied to the spin polarization of the 2p and 3p orbitals (Figure 4b,d). The polarization of $2s^\alpha$, $3s^\alpha$, and $3d^\alpha$ orbitals is of course not an isolated process but is accompanied by the polarization of all other orbitals of either spin. Besides the exchange interaction, Coulomb repulsion and electron−nucleus attraction also come into play. This will be discussed in more detail below.

The requirement of orthogonality between the 3s and 2s orbitals helps us also to understand better the dependence of their contributions to ρ_N on nuclear charge. From the orthogonality of $2s^\alpha_U(r)$ and $3s^\alpha_U(r)$ follows:

$$\langle 2s^\alpha_U(r)|3s^\alpha_U(r)\rangle = \langle 2s_R(r)|2s_R(r)\rangle + \langle 2s_R(r)|\Delta 3s^\alpha(r)\rangle + \langle \Delta 2s^\alpha(r)|3s_R(r)\rangle + \langle \Delta 2s^\alpha(r)|\Delta 3s^\alpha(r)\rangle = 0 \quad (11)$$

The first term in the middle of (11) vanishes, since the ROHF 2s and 3s orbitals are also orthogonal. The fourth term is negligible with respect to the second and third terms, since $\Delta 2s^\alpha(r)$

Table 4. Exchange, Coulomb, and Radial Overlap Integrals between the SOMO and the Doubly Occupied Orbitals for $^6Mn^{2+}$ (au)[a]

exchange integrals	1s	2s	Σ2p	3s	Σ3p
$\langle\psi_R 3d_R\|3d_R\psi_R\rangle$	0.000 278	0.026 949	0.079 875	0.081 590	0.298 482
$\langle\psi_U^\alpha 3d_R\|3d_R\psi_U^\alpha\rangle$	0.000 278	0.027 109	0.080 715	0.081 478	0.298 100
$\langle\psi_U^\alpha 3d_U^\alpha\|3d_U^\alpha\psi_U^\alpha\rangle$	0.000 278	0.027 172	0.080 900	0.081 553	0.298 340
$\langle\psi_U^\alpha 3d_U^\alpha\|3d_U^\alpha\psi_U^\alpha\rangle - \langle\psi_R 3d_R\|3d_R\psi_R\rangle$	0.000 000	0.000 223	0.001 025	−0.000 037	−0.000 142
$5\sum_\psi -[\langle\psi_U^\alpha 3d_U^\alpha\|3d_U^\alpha\psi_U^\alpha\rangle] - \langle\psi_R 3d_R\|3d_R\psi_R\rangle] = -0.005\,345$					

Coulomb integrals	1s	2s	Σ2p	3s	Σ3p
$\langle\psi_R 3d_R\|\psi_R 3d_R\rangle$	1.181 876	1.163 092	3.503 115	0.926 861	2.714 807
$\langle\psi_U^\alpha 3d_R\|\psi_U^\alpha 3d_R\rangle$	1.181 876	1.162 929	3.502 484	0.927 437	2.720 802
$\langle\psi_U^\alpha 3d_U^\alpha\|\psi_U^\alpha 3d_U^\alpha\rangle$	1.182 956	1.163 962	3.505 616	0.927 996	2.722 392
$\langle\psi_U^\beta 3d_U^\alpha\|\psi_U^\beta 3d_U^\alpha\rangle$	1.182 956	1.164 224	3.506 621	0.926 797	2.709 494

radial overlap integrals	1s	2s	2p	3s	3p
$\langle\psi_R\|3d_R\rangle$[b]	0.001 854	0.028 223	0.025 459	0.069 239	0.072 500
$\langle\psi_U^\alpha\|3d_R\rangle$[b]	0.001 855	0.028 413	0.025 748	0.069 099	0.072 259
$\langle\psi_U^\alpha\|3d_U^\alpha\rangle$[b]	0.001 857	0.028 444	0.025 776	0.069 116	0.072 272

nuclear attraction integrals	1s	2s	2p	3s	3p
$\langle\psi_R\|Z/r\|\psi_R\rangle$	612.889 503	131.448 180	129.454 856	40.539 902	37.291 698
$\langle\psi_U^\alpha\|Z/r\|\psi_U^\alpha\rangle$	612.885 311	131.191 339	129.169 607	40.713 359	37.617 042
$\langle\psi_U^\beta\|Z/r\|\psi_U^\beta\rangle$	612.892 007	131.627 837	129.643 564	40.433 853	37.032 423
	3*d*				
$\langle\psi_R\|Z/r\|\psi_R\rangle$	29.548 909				
$\langle\psi_U^\alpha\|Z/r\|\psi_U^\alpha\rangle$	29.575 906				

[a] Comparison of ROHF and UHF data. All radial wave functions have been normalized to $1/(4\pi) = 0.079\,577\,4$; see ref 30. [b] $\langle\psi|\varphi\rangle = \int\psi(r)^*\varphi(r)\, r^2\, dr$, where $\psi(r)$ and $\varphi(r)$ are radial parts of the orbitals $\psi(\mathbf{r},\sigma)$and $\varphi(\mathbf{r},\sigma)$, respectively.

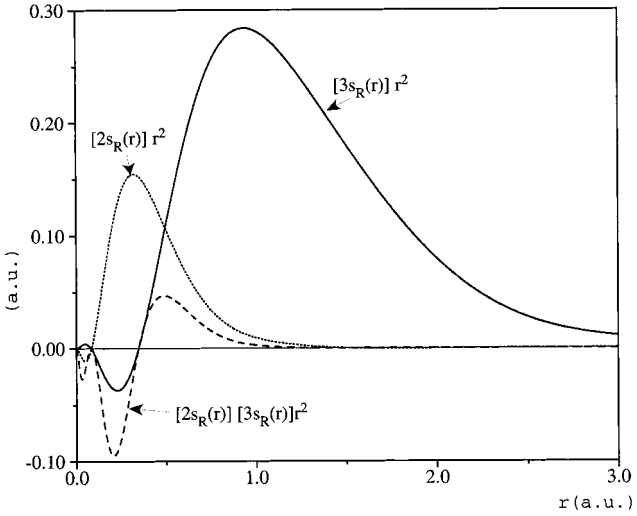

Figure 5. Orthogonality of 2s and 3s orbitals in Mn^{2+} (ROHF result). The function $f = 2s(r)3s(r)r^2$ integrates to zero. For comparison, the functions $2s(r)r^2$ and $3s(r)r^2$ are also shown. For 2s, the phase convention differs from that used elsewhere.[36]

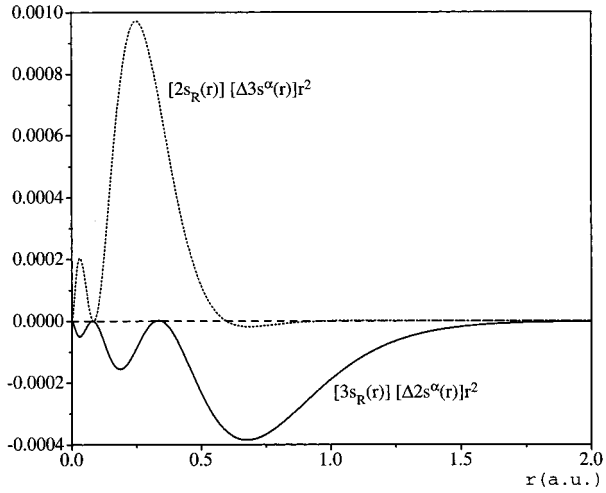

Figure 6. Consequences of the orthogonality between 2s and 3s orbitals in Mn^{2+}. The function $\Delta 2s^\alpha(r)3s_R(r)r^2 + \Delta 3s^\alpha(r)2s_R(r)r^2$ integrates to zero; see text.

$<< 2s_R(r)$ and $\Delta 3s^\alpha(r) << 3s_R(r)$. Hence,

$$\langle 2s_R(r)|\Delta 3s^\alpha(r)\rangle + \langle \Delta 2s^\alpha(r)|3s_R(r)\rangle \approx 0 \qquad (12)$$

Analogously, it may be shown that

$$\langle 2s_R(r)|\Delta 3s^\beta(r)\rangle + \langle \Delta 2s^\beta(r)|3s_R(r)\rangle \approx 0 \qquad (13)$$

Figure 6 illustrates eq 12 for Mn^{2+}. The function $\Delta 3s^\alpha(r)2s_R(r)r^2$ is positive at most *r* values, as $2s_R(r)$ and $\Delta 3s^\alpha$ have equal sign where they overlap significantly. The function $\Delta 2s^\alpha(r)r^2$ is negative everywhere, as regions of negative $\Delta 2s^\alpha(r)$ always match those of positive $3s_R(r)$, and vice versa.[36] The total area under $\Delta 2s^\alpha(r)3s_R(r)r^2$ and under $\Delta 3s^\alpha(r)2s_R(r)r^2$ is calculated to be +0.000 238 and −0.000 238, respectively. The approximation in deriving eq 12 from eq 11 appears thus to be well-justified. The spin polarization contributions

(36) Molecular or atomic orbitals are unique except for a phase factor. Unless noted otherwise, in this work all s-type orbitals are defined as to be positive at the nucleus. The choice of phase does not alter the physical mechanism.

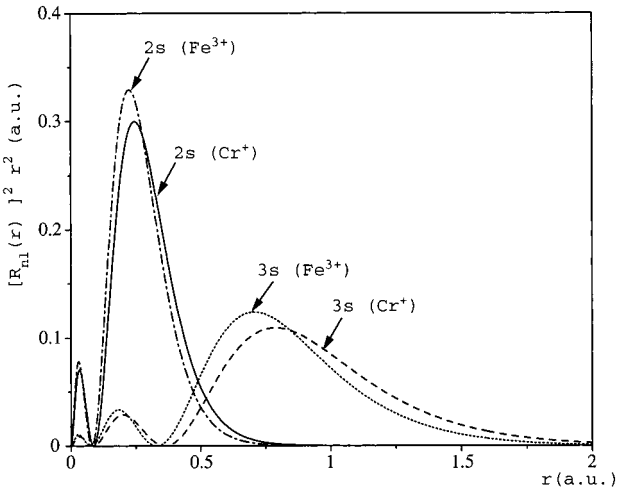

Figure 7. Effect of nuclear charge on the 2s and 3s orbitals. Comparison of $[2s(r)]^2r^2$ and $[3s(r)\ ]^2r^2$ for Cr^+ and Fe^{3+} (ROHF results).

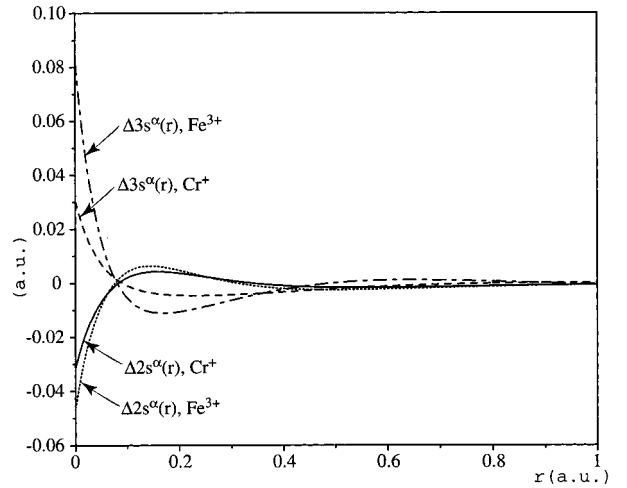

Figure 8. Core-shell spin polarization in Cr^+ and Fe^{3+}: $\Delta 2s^\alpha(r)$, $\Delta 3s^\alpha(r)$.

$\Delta 3s^\alpha(r)$ and $\Delta 2s^\alpha(r)$ have to match the restricted orbital distributions $2s_R(r)r^2$ and $3s_R(r)r^2$, to fulfill eq 12.

Figure 7 examines the changes in the ROHF 2s and 3s radial distributions upon increasing the nuclear charge by two (the d^5 ions $^6Cr^+$ and $^6Fe^{3+}$ are compared). Both 2s and 3s contract and increase their overlap with $\Delta 3s^\alpha$ and $\Delta 2s^\alpha$, respectively. The redistribution of the electron density is more pronounced for the more polarizable 3s orbital. This is seen most clearly when comparing the area confined between the curves $3s(Fe^{3+})$ and $3s(Cr^+)$ with the area confined between the curves $2s(Fe^{3+})$ and $2s(Cr^+)$. The contraction of 3s and 2s will thus enhance $\langle \Delta 2s^\alpha(r)|3s_R(r)\rangle$ more than $\langle \Delta 3s^\alpha(r)|2s_R(r)\rangle$. To retain orthogonality in the spin-polarized case, $\Delta 3s^\alpha(r)$ has to increase relative to $\Delta 2s^\alpha(r)$. This is supported by Figure 8: While the absolute value of $\Delta 2s^\alpha(r)$ increases only slightly from Cr^+ to Fe^{3+}, $\Delta 3s^\alpha(r)$ is significantly enhanced. Consequently, the ratio $\Delta 3s^\alpha(0)/\Delta 2s^\alpha(0)$ is larger for Fe^{3+}. Analogously, $\Delta 3s^\beta(0)/\Delta 2s^\beta(0)$ is enhanced. As a result, the magnitude of the 3s/2s ratio of core-shell spin polarization contributions to ρ_N increases with increasing nuclear charge (cf. Tables 2 and 3), due to the requirement of orthogonality between 2s and 3s shells.

Spin Polarization of the 1s **Orbital.** The direction of 1s spin polarization in Mn^{2+} is the same as for the 2s orbital: the α component expands, whereas the β component contracts. Both processes produce a negative contribution to ρ_N (cf. Tables 1 and 3). Previously the minimization of the electrostatic repulsion with the unpaired electrons had been considered to be the major driving force of the 1s spin polarization.[1,17] According to our calculation, 1s spin polarization does not lead to any significant difference between the α and β components with respect to exchange and Coulomb interaction with the SOMO, cf. Table 4.[37] From this, and from the small 1s contributions of either sign to ρ_N in different systems (Tables 1−3), we conclude that the 1s orbital reacts to the spin polarizations of the other doubly occupied orbitals rather than minimizing its repulsion with the SOMO. Note, for example, that the 1s contribution to ρ_N and the sum of the valence-shell contributions always have opposite signs (cf. also Tables 1 and 2).

Table 5. Analysis of ROHF and UHF Total Energies of $^6Mn^{2+}$ and ^4N (au)

	$^6Mn^{2+}$	^4N
$E_{tot,ROHF}$[a]	−1148.793 015	−54.398 026
$E_{tot,UHF}$[a]	−1148.795 003	−54.401 648
$E_{tot,UHF} - E_{tot,ROHF}$	−0.001 988	−0.003 622
$E_{kin,ROHF}$[b]	1148.959 337	54.397 176
$E_{kin,UHF}$[b]	1148.962 479	54.401 243
$E_{kin,UHF} - E_{kin,ROHF}$	0.003 142	0.004 067
$E_{pot,ROHF}$[c]	−2297.752 352	−108.795 202
$E_{pot,UHF}$[c]	−2297.757 482	−108.802 891
$E_{pot,UHF} - E_{pot,ROHF}$	−0.005 130	−0.007 689
$E_{Ne,ROHF}$[d]	−2717.979 039	−128.343 514
$E_{Ne,UHF}$[d]	−2718.011 143	−128.353 641
$E_{Ne,UHF} - E_{Ne,ROHF}$	−0.032 104	−0.010 127
$E_{ee,ROHF}$[e]	420.226 687	19.548 312
$E_{ee,UHF}$[e]	420.253 661	19.550 750
$E_{ee,UHF} - E_{ee,ROHF}$	0.0269 74	0.0024 38
$E_{C,ROHF}$[f]	511.200 248	31.975 583
$E_{C,UHF}$[f]	511.230 621	31.987 506
$E_{C,UHF} - E_{C,ROHF}$	0.030 373	0.011 923
$E_{X,ROHF}$[g]	−90.973 561	−12.427 271
$E_{X,UHF}$[g]	−90.976 960	−12.436 756
$E_{X,UHF} - E_{X,ROHF}$	−0.003 399	−0.009 485

[a] Total (kinetic + potential) energy of the system. [b] Total kinetic energy. [c] Total potential energy ($E_{pot} = E_{Ne} + E_{ee}$). [d] Total energy of the electrons due to nuclear attraction. [e] Total electron−electron repulsion energy ($E_{ee} = E_C + E_X$). [f] The sum of all Coulomb integrals, including self-interactions. [g] The sum of all exchange integrals, including self-interactions.

Spin Polarization and Energy Gain. The gain in exchange energy, due to spin polarization, between the five SOMOs and the doubly occupied orbitals in Mn^{2+} (−0.005 345 au; see Table 4) corresponds to 104% of the difference between the total UHF and ROHF potential energies (Table 5). For the ^4N atom, the corresponding gain in exchange energy represents 105% of the total reduction in potential energy (E_{pot}, Table 5). This is consistent with the usual interpretation of spin polarization as being due to improved exchange interactions between the SOMO(s) and the doubly occupied orbital(s) in the UHF wave function.

Additionally, the spin polarization creates a new equilibrium between electron−electron repulsion and electron−nuclear attraction. The crucial role of electron−nuclear attraction energy (E_{Ne}) is demonstrated in Table 5. It provides the main energy gain upon going from ROHF to UHF wave functions. This may be rationalized as follows: As the ROHF wave function is not relaxed with respect to exchange interactions between the SOMO and the other α spin−orbitals, the density is too diffuse. Spin polarization helps to contract the metal $3d^\alpha$, $3p^\alpha$, and $3s^\alpha$ orbitals and thus enhances electron−nuclear attraction. Part of this energy gain is compensated by the decontraction of the

(37) The strongly localized 1s shell experiences ~2 orders of magnitude less exchange interactions with 3d than 2s does.

charge density in $1s^{\alpha}$, $2s^{\alpha}$, $2p^{\alpha}$, as well as in $3s^{\beta}$ and $3p^{\beta}$ ($1s^{\beta}$, $2s^{\beta}$, $2p^{\beta}$ contract and thus lower E_{Ne}). Tables 4 and 5 show that the spin polarization improves exchange (E_X) but increases the total E_{ee}. This is also a consequence of an overall more contracted charge density. Nevertheless, E_{pot} decreases, due to the large contribution from E_{Ne}. The total kinetic energy (E_{kin}) increases, in agreement with the virial theorem.[38]

Table 4 also shows that, due to formal similarity, the exchange integrals and their changes upon spin polarization are closely connected with the radial overlap of the corresponding orbitals. (a) The exchange interaction increases in the series (3d,1s), (3d,2s) and (3d,3s) and so does the radial overlap; (b) the spin polarization increases the exchange integral with the SOMO when the radial overlap with the SOMO increases and vice versa.[39] In contrast, the Coulomb interaction increases along the series (3d,3s), (3d,2s), and (3d,1s), even though the 2s and particularly the 1s maximums are far from the 3d maximum. This implies that $\langle 1/r_{12}\rangle$ may actually increase with increasing distance between the radial maximums and vice versa. Compared to the 1s wave function, the 3s wave function occupies a larger angular space. Thus, the electrons in 3s and 3d orbitals are on average further apart (despite the large overlap of the corresponding radial wave functions).

Coming back to the historical interpretations of spin polarization in transition metal systems (section 2[1,15]), we conclude that the expansion of the $2s^{\alpha}$ orbital reduces its electrostatic repulsion with the SOMO, both by reduced Coulomb interaction (angular correlation) and by improved exchange (radial correlation). This would correspond to the usual "effective attraction" of like-spin electrons on a radial scale. On the other hand, the boundary condition of orthogonality to 2s forces the 3s spin polarization (expansion of $3s^{\alpha}$, contraction of $3s^{\beta}$), irrespective of the resulting partial energy loss.

Comparison to the Main-Group Case (^{4}N). The quartet ground state of the nitrogen atom is a good main-group example to be compared with, as it exhibits a spherical distribution of the three unpaired electrons in the 2p orbitals. The positive 2s contribution to ρ_N (0.91 au, UHF result) overcompensates the negative 1s contribution (−0.74 au), giving an overall positive ρ_N (cf. ref 19e). The spin polarization of the nitrogen 1s and 2s orbitals (Figure 2a,b) may be compared to the polarization of the 2s and 3s orbitals in Mn^{2+} (Figure 4a,c). For nitrogen, the $1s^{\alpha}$ and $2s^{\beta}$ orbitals expand, whereas the $1s^{\beta}$ and $2s^{\alpha}$ orbitals contract. Note that, in contrast to the situation for the 3s and 3d orbitals in Mn^{2+} (see above), the second maximum of the 2s distribution is located at slightly larger radius than the 2p maximum.

The opposite direction of the polarization of the $1s^{\alpha}$ and $2s^{\alpha}$ orbitals is again required by their mutual orthogonality. However, in contrast to the Mn^{2+} case, in this case, the spin polarization enhances the exchange interaction with the 2p SOMO for both s orbitals, despite the slight decrease of radial overlap between $2s^{\alpha}$ and $2p^{\alpha}$ (Table 6). This appears to be due to the dominant role of the second maximum of $2s^{\alpha}$. Spin polarization brings the latter closer to the $2p^{\alpha}$ maximum and thus enhances $2s^{\alpha}/2p^{\alpha}$ exchange. The acccompanying increase in $2s^{\alpha}/2p^{\alpha}$ Coulomb repulsion is compensated by reduced $2s^{\beta}/2p^{\alpha}$ repulsion and increased nuclear−electron attraction (Table 6).

Table 6. Exchange, Coulomb, and Radial Overlap Integrals between the SOMO and the Doubly Occupied Orbitals for ^{4}N (au)[a]

exchange integrals	1s	2s
$\langle\psi_R 2p_R\|2p_R\psi_R\rangle$	0.028 820	0.137 305
$\langle\psi_U^{\alpha} 2p_R\|2p_R\psi_U^{\alpha}\rangle$	0.029 190	0.138 789
$\langle\psi_U^{\alpha} 2p_U^{\alpha}\|2p_U^{\alpha}\psi_U^{\alpha}\rangle$	0.029 505	0.139 322
$\langle\psi_U^{\alpha} 2p_U^{\alpha}\|2p_U^{\alpha}\psi_U^{\alpha}\rangle - \langle\psi_R 2p_R\|2p_R\psi_R\rangle$	0.000 685	0.002 017
$3\Sigma_\phi - [\langle\psi_U^{\alpha} 2p_U^{\alpha}\|2p_U^{\alpha}\psi_U^{\alpha}\rangle - \langle\psi_R 2p_R\|2p_R\psi_R\rangle] = -0.008\ 106$		

Coulomb integrals	1s	2s
$\langle\psi_R 2p_R\|\psi_R 2p_R\rangle$	0.947 366	0.668 210
$\langle\psi_U^{\alpha} 2p_R\|\psi_U^{\alpha} 2p_R\rangle$	0.947 209	0.677 922
$\langle\psi_U^{\alpha} 2p_U^{\alpha}\|\psi_U^{\alpha} 2p_U^{\alpha}\rangle$	0.951 949	0.680 044
$\langle\psi_U^{\beta} 2p_U^{\alpha}\|\psi_U^{\beta} 2p_U^{\alpha}\rangle$	0.952 208	0.655 545

radial overlap integrals[b]	1s	2s
$\langle\psi_R\|2p_R\rangle$[b]	0.020 783	0.076 279
$\langle\psi_U^{\alpha}\|2p_R\rangle$[b]	0.021 107	0.075 845
$\langle\psi_U^{\alpha}\|2p_U^{\alpha}\rangle$[b]	0.021 217	0.075 882

nuclear attraction integrals	1s	2s
$\langle\psi_R\|Z/r\|\psi_R\rangle$	46.584 427	7.532 656
$\langle\psi_U^{\alpha}\|Z/r\|\psi_U^{\alpha}\rangle$	46.467 873	7.803 738
$\langle\psi_U^{\beta}\|Z/r\|\psi_U^{\beta}\rangle$	46.669 016	7.201 735
	2p	
$\langle\psi_R\|Z/r\|\psi_R\rangle$	6.703 116	
$\langle\psi_U^{\alpha}\|Z/r\|\psi_U^{\alpha}\rangle$	6.737 093	

[a] ROHF and UHF results. [b] See also corresponding footnote to Table 4.

Valence-Shell Spin Polarization in Mn^0. As a first step toward a better understanding of valence-shell spin polarization in transition metal systems, we examine the spin polarization of the 4s orbital in the $^6Mn^0$ atom, comparing ROHF and UHF wave functions and energies. The spin polarization is qualitatively the same as discussed above for the 2s orbital in nitrogen: The α-component contracts, whereas the β component expands (Figure 9). The exchange interaction between 3d and 4s (0.006 581 au at the ROHF level) is overall less pronounced than between 2s and 3d in Mn^{2+} (0.026 949 au; cf. Table 4), but the energy gain upon spin polarization is still significant (+0.000 872 au). This is due to the large polarizability of the 4s shell, which also leads to a significant redistribution of spin density (Figure 9) and to a larger spin polarization contribution to ρ_N from 4s compared to 3s (Table 1). We may also view this, within a configuration−interaction framework,[40] as a consequence of the lower excitation energies of the 4s valence compared to the 3s core orbital (for the same reason, spin contamination is largely connected to valence-shell spin polarization; see below). The same argument holds of course for the comparison between valence-shell 2s vs core-shell 1s spin polarization in nitrogen (see above).

6. Valence-Shell Spin Polarization in Molecules

As discussed above, the spin polarization of the core shells does not depend much on the particular bonding situation. It is similar for molecules and for atomic systems (cf. Tables 1 and

(38) Levin, I. N. *Quantum Chemistry*; Allyn and Bacon: Boston, 1975; p 363.

(39) Exchange interactions are more short-ranged than Coulomb repulsion and thus parallel more closely the radial overlap (see, e.g., Bethe, H. A.; Jackiw, R. *Intermediate Quantum Mechanics*; W. A. Benjamin, Inc.: Reading, MA, 1974). In contrast, Coulomb repulsion may also be large for two nonoverlapping pointlike charge distributions, provided their distance is not too large. Of course, even the exchange interactions may deviate from the behavior of the radial overlap integrals, due to the influence of the r_{12}^{-1} factor in the integrand of eq 4 (cf. also discussion for ^{4}N).

(40) Melchior, M. T., *J. Chem. Phys.* **1969**, *50*, 511.

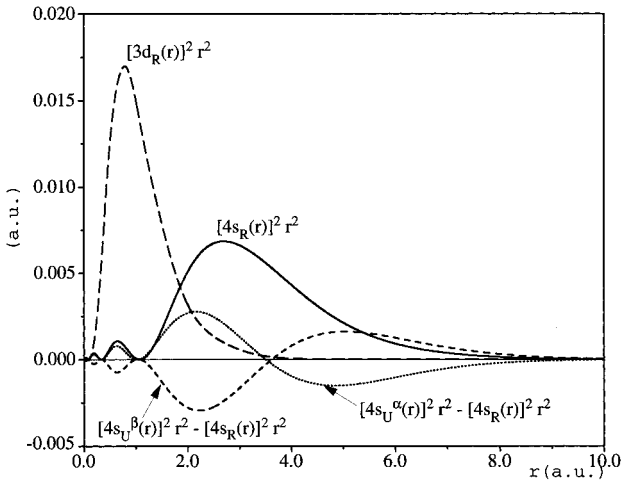

Figure 9. ROHF radial distribution function $[R_{nl}(r)]^2r^2$ (scaled by $^1/_4$.) and difference between ROHF and UHF radial distributions for the 4s orbital in Mn^0. For comparison, the radial distribution function of the 3d SOMOs (scaled by $^1/_4$.) is also plotted.

Table 7. Orbital Contributions to A_{dip} for TiF_3 and MnO_3 (au)[a]

		contribution	
MO	character	TiF_3	MnO_3
$7a_1'$	(metal $3d_z^2$ +4s, singly occupied MO)	0.441	0.640
$3a_2''$	(ligand $2p_z$)	0.012	0.052
$1e''$	(metal $3d_{xz}$, $3d_{yz}$; ligand $2p_z$)	0.005	0.147
$6a_1'$	(metal 4s, 3 d_z^2; ligand $2p_x$, $2p_y$)	0.013	0.206
$5e'$	(metal $3d_{xy}$, $3d_{x^2-y^2}$; ligand $2p_x$, $2p_y$)	−0.014	−0.113
$4e'$	(ligand 2s)	0.051	0.008
$2a_2'$	(metal $3p_z$)	−0.086	−0.018
$3e'$	(metal $3p_x$, $3p_y$)	−0.108	−0.152
$1a_2''$	(metal $2p_z$)	−0.067	−0.143
$2e'/1e'$	(metal $2p_x$, $2p_y$)	0.048	0.108
total		0.305	0.746
exp		0.22(1)...0.0.27(1)[b]	0.62(2)[b]
$<S^2>$		0.7526	0.7875

[a] DFT(BP86) results. All values have been divided by the nuclear *g* value. Contributions, which were for both molecules smaller than 0.01 au, have been omitted. [b] Reference 11.

2). In contrast, the spin polarization of the valence shells is characteristic of the specific chemical environment and bonding. We have selected the four examples, TiF_3, MnO_3, $[Mn(CO)_5]$, and $[Mn(CN)_4N]^-$, to discuss valence-shell spin polarization contributions to ρ_N. DFT results obtained with the BP86 functional will be examined (Tables 1 and 2).

These complexes represent a variety of different bonding situations (cf. Tables 7 and 8 for a characterization of the MOs). TiF_3[22] and MnO_3 are isoelectronic, trigonal planar (D_{3h}) d^1 complexes. Their SOMO ($7a_1'$) is metal−ligand σ antibonding and is dominated by the metal $3d_z^2$ orbital, with some 4s character mixed in. While the SOMO in TiF_3 is localized to 94% at the metal (with 76% $3d_z^2$, and 18% 4s character[41]), in MnO_3 it is more delocalized (with 49% $3d_z^2$, 15% 4s, and 36% ligand character). Three σ-bonding orbitals ($5e'$, $6a_1'$) are formed by the interaction of metal $3d_{xy}$ and $3d_{x^2-y^2}$ orbitals (e'), a metal $3d_z^2$ orbital with 4s admixture (a_1'), and the appropriate ligand orbital combinations. In addition, two partial π bonds are formed by an interaction of the metal $3d_{xz}$ and $3d_{yz}$ orbitals with the appropriate linear combination of ligand $2p_z$ orbitals ($1e''$). The third linear combination of ligand $2p_z$ orbitals is nonbonding ($3a_2''$). $[Mn(CO)_5]$ and $[Mn(CN)_4N]^-$ adopt square-pyramidal structures (C_{4v} symmetry). $[Mn(CO)_5]$ is a low-spin d^7 complex. Its SOMO is composed of metal $3d_z^2$ and $4p_z$ orbitals ($17a_1$). The $4p_z$ admixture reduces the σ-antibonding interaction with the axial ligand by polarizing the SOMO toward the opposite side. The metal 4s contribution to the SOMO is small, giving a small, positive direct SOMO contribution to ρ_N. $[Mn(CN)_4N]^-$ is a d^1 complex with a single metal $3d_{xy}$-type SOMO ($2b_1$). In both square-pyramidal complexes, two σ bonds in the equatorial plane are formed by an interaction between a metal $4s/3d_z^2$ hybrid, the metal $3d_{x^2-y^2}$ orbital, and the corresponding ligand σ-bonding hybrids (a_1 and b_2 MOs). The σ bond to the axial ligand involves mainly the metal $3d_z^2$ orbital. The metal $3d_{xy}$ orbital (b_1) is partially π bonding to the equatorial ligands, the $3d_{xz}$, $3d_{yz}$ orbitals (e) interact also with the axial ligand. The antibonding counterparts of the latter three orbitals (which may be derived from the well-known t_{2g} set in octahedral symmetry) correspond to the six nonbonding d electrons of $[Mn(CO)_5]$.

The valence-shell spin polarization concentrates α spin density at the metal (cf. discussion above for the Mn^0 atom and ref 18). An excess of β spin density is left at the ligands. In $[Mn(CN)_4N]^-$, the spin polarization increases the atomic spin population of Mn from 0.51 (SOMO contribution) to 1.18 (total spin population[41]). The α spin density is withdrawn mainly from the axial ligand and added mainly to d-type orbitals of Mn (0.25, 0.10, 0.10, 0.07, and 0.06 electrons to d_{xy}, d_{xz}, d_{yz}, $d_{x^2-y^2}$, and d_z^2, respectively). This likely enhances the overall negative core-shell spin polarization contributions to ρ_N (cf. section 5). The spin population of the 4s orbital increases also slightly (several metal−ligand bonding orbitals are involved), resulting in a small contribution to ρ_N of +0.04 au (Table 1). This is much less than the valence-shell contribution in Mn (+0.93 au), where the spin polarization of the fully occupied 4s orbital contributes (note also that $[Mn(CN)_4N]^-$ has only one unpaired electron whereas Mn has five).

Similarly, spin polarization increases the spin population at the metal in $Mn(CO)_5$ from 0.58 (SOMO contribution) to 0.82. The increase concentrates mostly in orbitals of e symmetry (the metal $3d_{xz}$, $3d_{yz}$, $4p_x$, and $4p_y$ orbitals, total gain ∼0.13). The spin population in orbitals of a_1 symmetry increases only slighly, by 0.04 for $3d_z^2$ and by 0.03 for 4s. The increase is only 0.03 and 0.01 for $3d_{xy}$ and $3d_{x^2-y^2}$, respectively (with significant consequences for A_{dip}, cf. below).

Negative valence-shell contributions to ρ_N are found for the isoelectronic TiF_3 and MnO_3, due to an interesting rehybridization mechanism: The spin polarization, mainly of the metal−ligand σ-bonding $6a_1'$ MO, shifts α density from the ligands toward the metal. Therefore, the spin population at the metal is enhanced from 0.93 (SOMO contribution) to 1.04 in TiF_3, and from 0.64 to 1.19 in MnO_3 (the larger effect for the manganese complex is a consequence of the larger covalence of the σ bonds). However, at the same time, the metal contribution to this bonding MO loses 4s character and gains 3d character. Therefore, the overall valence-shell spin polarization contribution to ρ_N and thus to A_{iso} is negative (and that to A_{dip} positive, cf. below), in particular for the very covalent MnO_3. We also note that, in TiF_3, the excess α spin density is distributed almost equally over all five metal d orbitals. In contrast, the excess spin population in MnO_3 pertains mostly to the d_z^2, d_{xz}, and d_{yz} orbitals (+0.17, +0.13, and +0.13, respectively) and less to the d_{xy} and $d_{x^2-y^2}$ orbitals (each +0.05).

(41) The orbital compositions and spin populations reported here have been obtained using a Mulliken population analysis of the BP86 Kohn−Sham wave function.

Table 8. Orbital Contributions to A_{dip} for $[Mn(CO)_5]$ and $[Mn(CN)_4N]^-$ (au)[a]

MO in $[Mn(CN)_4N]^-/[Mn(CO)_5]$	character	contribution $[Mn(CN)_4N]^-$	contribution $[Mn(CO)_5]$
$-/17a_1$	(Mn $3d_z^2$, $4p_z$, 4s, SOMO in $[Mn(CO)_5]$)		0.763
$-/11e$	(Mn $3d_{xz}$, $3d_{yz}$; eq ligands $2p_z$)		0.032
$2b_1/2b_1$	(Mn $3d_{xy}$, eq lig $2p_x$, $2p_y$, SOMO in $[Mn(CN)_4N]^-$)	−0.669	−0.040
$13a_1/14a_1$	(eq ligands sp_x, sp_y hybrids; Mn 4s)	−0.030	0.002
$5b_2/5b_2$	(eq ligands sp_x, sp_y hybrids; Mn $3d_{x^2-y^2}$)	−0.015	0.000
$1b_1/1b_1$	(Mn $3d_{xy}$, eq ligands $2p_x$, $2p_y$)	−0.273	−0.003
6e/10e	(Mn $3d_{xz}$, $3d_{yz}$; eq ligands $2p_x$, $2p_y$)	0.110	0.021
$4b_2/6b_2$	(Mn $3d_{x^2-y^2}$, eq ligands $2s+2p_x+2p_y$)	−0.069	−0.013
$11a_1/12a_1$	(Mn $4s+3d_z^2$, eq ligands $2s+2p_x+2p_y$)	0.018	−0.002
$8a_1/9a_1$	(Mn $3p_z$)	0.076	0.057
4e/4e	(Mn $3p_x$, $3p_y$)	−0.121	−0.044
$3a_1/3a_1$	(Mn $2p_z$)	−0.077	−0.094
1e/1e	(Mn $2p_x$, $2p_y$)	0.163	0.048
total		−0.882	0.727
exp		−0.929[b]	0.68(6),[b] 0.70(5)[b]
$<S^2>$		0.7729	0.7544

[a] DFT(BP86) results. See also footnote to Table 7. [b] Reference 11.

In both $[Mn(CN)_4N]^-$ and MnO_3, the largest valence-shell spin polarization is experienced by doubly occupied orbitals which are the bonding counterparts of the partly antibonding SOMO (this holds at the BP86 level but is altered upon adding Hartree−Fock exchange; see section 8). In $[Mn(CN)_4N]^-$, this is the $1b_1$ orbital which represents π bonding between the metal and the equatorial ligands. In MnO_3 it is the σ-bonding $6a_1'$ orbital. This observation may again be rationalized by a tendency to maximize the exchange interaction with the SOMO; i.e., the α component of the doubly occupied MO is polarized toward the metal (where the SOMO is largely localized), the β component toward the ligands. Due to the large overlap with the SOMO, the spin polarization is particularly effective in these MOs. The abovementioned rehybridization in the α and β components of the σ-bonding $6a_1'$ MO of MnO_3 and TiF_3 may be understood analogously: The SOMO has more $3d_z^2$ than 4s character, and thus an increase of the relative d character in the α component of the bonding MO improves the exchange interaction with the SOMO. In TiF_3 and $Mn(CO)_5$, the bonding counterparts of the (antibonding) SOMO are not polarized significantly. In TiF_3, this is due to the ionic character of the bonds. In $Mn(CO)_5$, the SOMO is polarized away from the ligands (by $4p_z$ admixture) and thus has also little overlap with the doubly occupied valence MOs.

7. Effect of Spin Polarization on Dipolar Coupling Constants

While spin polarization is usually not considered for the dipolar hyperfine coupling (cf. Introduction), two recent computational studies have shown that in transition metal systems spin polarization may have a significant influence.[11,22] The most important MO contributions to the metal dipolar couplings of our four example systems are summarized in Tables 7 and 8 (again, DFT results with the BP86 functional are compared). As expected, the largest contribution in all cases is the direct one from the SOMO. This is positive for TiF_3, MnO_3, and $[Mn(CO)_5]$ but negative for $[Mn(CN)_4N]^-$.[42] However, contributionsdue to the spin polarization of the doubly occupied orbitals are clearly nonnegligible. We may discriminate again between core- and valence-shell spin polarization.

Core-Shell Spin Polarization. A common feature of all four systems are the significant contributions to A_{dip} from metal p-type core orbitals. The metal $2p_z$ contributions are always negative; the $2p_x$ and $2p_y$ contributions are always positive. This is consistent with the discussion in section 5: Spin polarization expands the $2p^\alpha$ orbitals and contracts the $2p^\beta$ orbitals. Thus, the positive contribution from $2p_z^\alpha$ to A_{dip} becomes smaller than the negative one from $2p_z^\beta$, and the negative contributions from $2p_x^\alpha$, $2p_y^\alpha$ become smaller than the positive ones from $2p_x^\beta$, $2p_y^\beta$. In a system of cubic or higher symmetry, these contributions would cancel exactly. In less symmetric systems, the anisotropy of the 2p spin polarization disturbs the balance between the two contributions. For our four systems, the effect is clearly nonnegligible, corresponding to ∼5−10% of the total A_{dip}. The $2p_z$ orbital dominates the 2p shell contributions in TiF_3, MnO_3, and $[Mn(CO)_5]$ (the $3d_z^2$-type SOMO affects particularly the $2p_z^\alpha$ component), whereas spin polarization contributions from $2p_x$ and $2p_y$ orbitals are larger in $[Mn(CN)_4N]^-$ (the $3d_{xy}$-type SOMO affects mostly $2p_x^\alpha$ and $2p_y^\alpha$).

The requirement of orthogonality between the 3p and 2p shells for atoms, as stated in section 5, does not hold strictly for molecules. Nevertheless, the $3p_x$ and $3p_y$ contributions to A_{dip} generally have the opposite sign of the $2p_x$ and $2p_y$ contributions. The $2p_z$ and $3p_z$ contributions are also of opposite sign for $[Mn(CO)_5]$ and $[Mn(CN)_4N]^-$. Therefore, the positive $3p_z$ and the negative $3p_x$ and $3p_y$ contributions partially cancel, leading to a relatively low overall 3p contribution. In TiF_3 and MnO_3, the presence of the d_z^2-type SOMO forces both $2p_z^\alpha$ and $3p_z^\alpha$ orbitals to expand. Therefore, $3p_z$ and $3p_x/3p_y$ contributions do not compensate but enhance each other. Therefore, the spin polarization contributions from the 3p shell in TiF_3 and MnO_3 are particularly large and amount to ∼23% of the total A_{dip} in MnO_3 and even to ∼64% in TiF_3![11,22]

Valence-Shell Spin Polarization. In the relatively ionic complex TiF_3, valence-shell spin polarization contributions to A_{dip} are small, with the largest individual MO contribution arising from a nonbonding fluorine 2s orbital combination of 4e′ symmetry (this and other results of our analysis for TiF_3 are consistent with earlier results by Belanzoni et al.[22]). We find larger valence-shell contributions for MnO_3 (Table 7). The covalency of the Mn−O σ and π bonds enables a significant

(42) The dipolar hyperfine interaction is a vector property and depends on the orientation of the orbitals involved. For a single α electron in a d_z^2 orbital, the (A_{xx},A_{yy},A_{zz}) vector is of the form $(-B,-B,+2B)$. For the other d orbitals, the signs are reversed. For $d_{x^2-y^2}$ $(A_{xx},A_{yy},A_{zz}) \approx (B, B,-2B)$, for d_{xz} $(A_{xx},A_{yy},A_{zz}) \approx (B, -2B, B)$, and so on. Analogous considerations hold for p orbitals. For p_z $(A_{xx},A_{yy},A_{zz}) \approx (-B,-B,+2B)$, for p_x $(A_{xx},A_{yy},A_{zz}) \approx (+2B,-B,-B)$, and for p_y $(A_{xx},A_{yy},A_{zz}) \approx (-B,2B,-B)$. See, e.g., ref 2 for a detailed discussion.

shift of α spin density toward the metal (cf. above). Large positive contributions to A_{dip} arise from the 6a′ and 1e″ MOs (involving the metal d_z^2 and d_{xz}/d_{yz} orbitals, respectively), whereas the 5e′ MO (involving the metal d_{xy} and $d_{x^2-y^2}$ orbitals) contributes negatively. Thus, while the overall negative spin polarization contributions to A_{dip} in TiF_3 involve mainly the core shells (in particular 3p), additional significant, overall positive valence-shell contributions dominate for the more covalent MnO_3. This has consequences for the sensitivity to spin contamination (see below).

Valence-shell spin polarization contributions to A_{dip} in $[Mn(CO)_5]$ are relatively small and partially compensate each other (Table 8). This appears to be a direct consequence of the character of the SOMO, which overlaps very little with the other valence MOs. In contrast, valence-shell contributions in $[Mn(CN)_4N]^-$ are significant. The largest contribution arises from the energetically high-lying, doubly occupied counterpart ($1b_1$) of the $2b_1$ SOMO. If it were not for its very large, negative contribution, the remaining valence-shell spin polarization contributions would almost cancel each other: A significant positive contribution from the π bonding 6e MO is compensated by negative contributions from equatorially σ-bonding MOs. The significant valence-shell spin polarization contribution to A_{dip} (29% of the total value) in $[Mn(CN)_4N]^-$ is thus at least in part due to the presence of a doubly occupied MO that has particularly large overlap with the SOMO.

8. Spin Polarization and Spin Contamination

The above discussion shows clearly that the two complexes MnO_3 and $[Mn(CN)_4N]^-$ exhibit particularly pronounced valence-shell spin polarization, due to the presence of high-lying doubly occupied bonding MOs that overlap strongly with the SOMO. These two systems were also two of the most critical cases in our systematic validation of different density functionals for the calculation of hyperfine coupling constants.[11] In particular, spin contamination turned out to be a problem when hybrid functionals were used. For $[Mn(CN)_4N]^-$, we found that the spin contamination was related to a mixing in of low-lying excited states that involve π-type orbitals. Upon going from a pure gradient-corrected ("GGA") functional like BP86 to hybrid functionals incorporating exact exchange, the population of each of the metal d_{xz} and d_{yz} orbitals increased dramatically, e.g., from 0.08 for BP86 to 0.62 for the "half-and-half" BHP86 functional. At the same time, the S^2 expectation value of the Kohn−Sham wave function[43] indicated a significant increase in spin contamination (BP86: $\langle S^2 \rangle = 0.773$; BHP86: $\langle S^2 \rangle = 1.784$). Similar effects were noted with MnO_3.[11] Obviously, the exact-exchange contribution to the hybrid functionals favors excited states of higher spin multipicity to the extent that the UKS wave functions for the ground state of these types of systems become significantly spin-contaminated.

In both systems, the description of A_{dip} deteriorated significantly with hybrid functionals, becoming too positive for MnO_3 and insufficiently negative for $[Mn(CN)_4N]^-$. Our present analysis indicates that the spin contamination produces too large spin populations in d_{xz}- and d_{yz}-type orbitals and thus too large positive contributions to A_{dip} from these orbitals. For similar reasons, hybrid functionals underestimated A_{dip} in the related complex $[Mn(CN)_5NO]^{2-}$.[11] At the same time, the isotropic coupling constants, i.e., the spin density at the metal nuclei, are also affected significantly by the spin contamination: As the spin population of metal d-type orbitals is exaggerated, the spin polarization of the 3s and 2s core shells becomes too large. Thus, for example, the core-shell spin polarization contribution to ρ_N in $[Mn(CN)_4N]^-$ increases from −0.192 au with the BP86 functional up to −0.566 au with the BHP86 functional (with very small changes in the valence-shell contributions). Consequently, the BHP86 result for A_{iso} (−558.5 MHz) is considerably more negative than the experimental value (−219.5 MHz). Note, in contrast, that for TiF_3 or $[Mn(CO)_5]$ no significant spin contamination was found,[11] consistent with the small valence-shell spin polarization (due to the small overlap between SOMO and doubly occupied valence MOs; see above).

9. Conclusions

The present study has shed light from various directions on hyperfine coupling in 3d transition metal complexes. From the detailed analysis of the spin polarization of the metal core shells in atomic systems, we have learned that the opposite contributions from the metal 2s and 3s shells to the spin density at the metal nucleus, ρ_N, and of the 2p and 3p shells to the dipolar coupling constants, A_{dip}, is a consequence of the orthogonality requirement between orbitals of the same angular momentum. While the 2s and 2p orbitals maximize their exchange interaction with the SOMO, the 3s and 3p orbitals are forced to lose some of their exchange to stay orthogonal to their respective penultimate shell. Changes of the ratio between 2s and 3s (and between 2p and 3p) contributions to ρ_N along the 3d series may be understood from the nodal structure of the orbitals. We expect that similar considerations apply to 4d and 5d systems.

Parts of this analysis are consistent with traditional views of spin polarization, e.g., in main-group compounds, as being due to enhanced exchange between the α component of the respective doubly occupied orbitals and the SOMO. A complete view, however, has to include the complementary polarization of the β spin−orbitals, as well as changes in Coulomb repulsion and nuclear−electron attraction.

While the core-shell spin polarization contributions to the isotropic hyperfine couplings have been found to be proportional to the spin population in the metal 3d orbitals, they are relatively independent of other details of the bonding. In contrast, the valence-shell spin polarization depends strongly on the electronic structure of the system. Particularly large valence-shell spin polarization contributions to both isotropic and dipolar coupling constants are found for systems in which the SOMO overlaps significantly with certain high-lying doubly occupied valence orbitals. These are the same cases in which our previous study[11] found dramatic spin contamination effects to plague unrestricted Kohn−Sham calculations with hybrid functionals. In addition to providing some basic insight into the mechanisms of spin polarization in transition metal systems, the results of the present work may also be used to pinpoint the weaknesses of certain theoretical approaches for the calculation of hyperfine couplings and thus hopefully also to develop improved methods.

In contrast to the assumptions implicit in many qualitative[2] and quantitative[44,45] schemes in current use by experimentalists, both core- and valence-shell spin polarization may significantly contribute to transition metal dipolar coupling constants. Moreover, for TiF_3 and MnO_3, we have identified an interesting 3d/4s rehybridization of the SOMO upon including spin

(43) These $\langle S^2 \rangle$ values pertain to the noninteracting reference system rather than to the real system. Such data are nevertheless expected to give a reasonable and useful representation for the real system as well (see, e.g.: Baker, J.; Scheiner, A.; Andzelm, J. *Chem. Phys. Lett.* **1993**, *216*, 380).

(44) Varberg, T. D., Field, R. W., Merer, A. J. *J. Chem. Phys.* **1991**, *95*, 1563.

(45) Balfour, W. J., Merer, A. J., Niki, H. *J. Chem. Phys.* **1993**, *99*, 3288.

polarization. These features complicate the extraction of spin densities and orbital character from experimental A_{dip} values. Explicit quantum chemical analyses are thus to be preferred instead.

Acknowledgment. This study has been supported by Deutsche Forschungsgemeinschaft and by Fonds der Chemischen Industrie. Part of this work benefitted also from the graduate college "Moderne Methoden der magnetischen Resonanz in der Materialforschung" at Universität Stuttgart. We are grateful to Drs. Dominik Munzar (Brno), Bernd Schimmelpfennig (Stockholm), and Vladimir Malkin (Bratislava) for helpful discussions.

JA002062V